Catalysis Today 155 (2010) 66–74

Contents lists available at ScienceDirect

Catalysis Today

journal homepage: www.elsevier.com/locate/cattod

Microreactor catalytic combustion for chemicals processing

Ahmet K. Avcı [a,*], David L. Trimm [b], Mustafa Karakaya [a]

[a] Department of Chemical Engineering, Boğaziçi University, Bebek 34342, Istanbul, Turkey
[b] CSIRO Petroleum, Private Bag 10, Clayton South, VIC 3169, Australia

ARTICLE INFO

Article history:
Available online 4 March 2009

Keywords:
Methanol synthesis
Ethane dehydrogenation
Microchannel reactors
Cascade reactors
Methane combustion
Methane steam reforming
Computational fluid dynamics

ABSTRACT

Comparison is drawn between two small reactor systems in the context of production of methanol from synthesis gas (syngas) and of ethylene by the non-oxidative dehydrogenation of ethane using computer-based modelling techniques. The production of methanol requires syngas containing hydrogen and carbon monoxide at controlled temperatures. The supply of syngas from a combination of steam reforming and catalytic combustion of methane was modelled for a parallel microchannel array and for a cascade reactor system in which reaction occurs in a series of beds, heat exchange in interconnecting microchannel heat exchangers being used to maintain the desired temperature. Although conversion was slightly higher in the microchannel systems, the advantages of better temperature control and easy replacement of deactivated catalyst favoured the cascade array. The use of the two reactor systems was also modelled for the ethane dehydrogenation, a reaction in which temperature control is essential to minimise coking. In this case catalytic combustion of methane provided direct heat to the dehydrogenation chamber. Again the microchannels gave slightly better conversion but temperature control was superior in the cascade system. The size of equipment needed to produce unit amount of product was smaller for the cascade systems in both cases, favouring their use for remote location operations.

1. Introduction

Although it is well known that the economies of scale favour large chemical plants, recent years have seen a growing interest in process intensification and microsystem technology. Chemical manufacturing systems that can be used in small scale and in distributed production are seen to have significant advantages such as reduced capital cost, smaller plant footprints and potentially easier transportation [1]. These advantages can be particularly valuable when considering the exploitation of remote resources such as offshore reserves of natural gas.

One of the basic building blocks of the developing microsystem technology has been the development of microchannel reactors, in which fine fluid passages having a characteristic size range of 10–1000 μm are cut into ceramic or metal plates, which are then being stacked and bonded to create the process modules at very high surface area-to-volume ratios up to ca. $5 \times 10^4\ m^2\ m^{-3}$ [2,3]. In case of catalytic systems, catalysts and supports can be coated on the microchannel walls to promote individual reactions [2–4]. Microchannel reactors for the steam reforming of natural gas are of particular interest in that the heat necessary to drive the endothermic reaction can be supplied by catalytic oxidation proceeding in a series of channels parallel to those in which reforming occurs [5–8]. The rate of heat transfer between these parallel channels can be very high as a result of the small channel sizes [3]. As a result, such systems are suitable for producing syngas which can be used as a chemical feedstock for reactions such as Fischer–Tropsch processing or methanol synthesis [9]. The latter reaction serves as a good example to illustrate their use.

Although they have significant beneficial features, microchannel reactors can have some disadvantages when their routine use in commercial practice, which is at its infancy, is considered. The catalysts buried in the microchannels cannot be easily replaced upon deactivation. Moreover, the small channels are subject to the risk of blockage due to effects such as carbon formation [10]. However, some of these difficulties can be avoided by the use of a second type of microchannel system, the cascade reactor array [11,12]. This system consists of multiple adiabatic beds containing catalysts linked by microchannels in which only heat exchange occurs. One set of reactors and microchannels are associated with the desired reaction (e.g. steam reforming) and one set with catalytic oxidation, the channels connecting the reactors being arranged parallel to the reforming channels in order to facilitate heat transfer. The concept of using catalytic reactor beds with interstage heat exchange to achieve higher conversions is a classic approach and has industrially established examples such as oxidation of SO_2 to SO_3. However, the cascade reactor system is novel since it employs microchannel technology in their heat

* Corresponding author. Tel.: +90 212 3597785; fax: +90 212 2872460.
E-mail address: avciahme@boun.edu.tr (A.K. Avcı).

0920-5861/$ – see front matter © 2009 Elsevier B.V. All rights reserved.
doi:10.1016/j.cattod.2009.01.046

Nomenclature

A_{cj}	cross-sectional area of reactors in exo- or endothermic line j (m^2)
c_{ij}	concentration of species i in channel j (mol m^{-3})
COMB	methane combustion (reaction (4))
C_{pi}	heat capacity of species i (J mol^{-1} K^{-1})
C_{pj}	heat capacity of gas mixture in channel j (J kg^{-1} K^{-1})
D	channel diameter (m)
$\mathcal{D}_{AB}$	species diffusivity (A into stagnant B) (m^2 s^{-1})
ED	ethane dehydrogenation (reaction (5))
F_{ij}	molar flow rate of species i along the operation line j (mol s^{-1})
F_{Tj}	total molar flow rate along the operation line j (mol s^{-1})
H	height of microchannel heat exchanger (m)
HC	hydrocarbon (CH_4 or C_2H_6)
$-\Delta H_k$	heat of reaction k (J mol^{-1})
L	microchannel length (m)
L_{rs}	wall thickness (m)
p_j	pressure in channel j (or along the operation line j) (atm)
Q_j	heat generated or consumed in washcoat j (J m^{-3} s^{-1})
r_j	radial coordinate in channel j (m)
r_k	rate of reaction k (mol kg_{cat}^{-1} s^{-1})
r_s	radial coordinate in the solid domain (m)
R_{ij}	rate of generation or depletion of species i in washcoat j (or along the operation line j) (mol m^{-3} s^{-1}) (mol kg_{cat}^{-1} s^{-1})
SR	methane steam reforming (reactions (1) and (2))
T	temperature (K)
T_j	temperature in channel j (or along the operation line j) (K)
U_j	plug-flow velocity into channel j (m s^{-1})
v_{rj}	radial component of velocity in channel j (m s^{-1})
v_{zj}	axial component of velocity in channel j (m s^{-1})
W	width of microchannel heat exchanger (m)
W_j	weight of catalyst used in each reactor in exo- or endothermic line j (kg_{cat})
x_{HC}	hydrocarbon conversion
x_S, y_S	solid wall coordinates (m)
z_j	axial coordinate in channel j (m)

Greek letters

$\in$	thickness of insulating layer (m)
$\in_p$	porosity of washcoat layer
κ	permeability of washcoat layer (m^2)
λ_j	thermal conductivity of gas mixture in channel j (W m^{-1} K^{-1})
λ_s	solid thermal conductivity (W m^{-1} K^{-1})
μ_j	gas viscosity in channel j (kg m^{-1} s^{-1})
ρ_{bj}	bulk density of catalyst in line j (kg_{cat} m^{-3})
ρ_j	gas density in channel j (kg m^{-3})

Subscripts

0	inlet quantity
eff	effective diffusivity or conductivity in the washcoat phase
i	species index
j	channel or cascade array index
k	reaction index
max	maximum
s	solid wall

exchangers and is an intensified version of an existing concept [11]. The design and operation of such systems for hydrogen production have been demonstrated by Seris et al. [11,12].

The cascade configuration has some advantages over the microchannel reactors. Catalyst, particulate or monolithic type, is placed in slots within a heat exchange block, thus avoiding the need to redistribute the reactants after each heat exchange and allowing facile replacement of deactivated catalyst. The heat transfer zone and catalyst volume are decoupled and can be independently varied. Furthermore, it is possible, by appropriate design, to inject reactants as the fluid passes through the series of multiple beds. The size of the cascade systems may be comparable to microchannel reactor arrays and is certainly smaller than the conventional plants [11,12]. The purpose of the present work is to explore the efficiency and size of cascade systems compared to the microchannel reactor arrays. This is done in the context of the production of methanol from natural gas and the non-oxidative dehydrogenation of ethane, both of which demand temperature control.

2. Description of the processes

The overall production of methanol from natural gas, represented by methane, involves two steps: the endothermic reforming of natural gas and the exothermic synthesis reaction [9]:

$$CH_4 + H_2O = CO + 3H_2 \qquad \Delta H^0_{298} = +206\ \text{kJ/mol} \tag{1}$$

$$CH_4 + 2H_2O = CO_2 + 4H_2 \qquad \Delta H^0_{298} = +165\ \text{kJ/mol} \tag{2}$$

$$CO + 2H_2 = CH_3OH \qquad \Delta H^0_{298} = -90.6\ \text{kJ/mol} \tag{3}$$

The desired heat to drive the endothermic reforming reactions is provided by catalytic combustion in either a microchannel system or a cascade reactor sequence:

$$CH_4 + 2O_2 = CO_2 + 2H_2O \qquad \Delta H^0_{298} = -802.3\ \text{kJ/mol} \tag{4}$$

The overall description of the methanol synthesis process is shown in Fig. 1. In the microchannel system, methane and steam are fed to the endothermic reformer which is heated by catalytic combustion of a second stream of methane. The reforming reactor is operated at about 1123 K to produce a gas suitable for the methanol synthesis (H_2:CO:CO_2 = 75:24:1 per cent by mole) [9]. Since reaction (3) will require only two moles of hydrogen per carbon monoxide, carbon dioxide coming from combustion (reaction (4)) can be injected into the methanol synthesis reactor (not considered in Fig. 1 and in modelling studies) to convert the excess hydrogen to a mixture of carbon monoxide and steam via the reverse water gas shift reaction ($CO_2 + H_2 = CO + H_2O$, $\Delta H^0_{298} = +41.2$ kJ/mol). Such a route can help in approaching the H_2:CO = 2 of reaction (3) and can therefore favour methanol formation. Copper-based catalysts used for synthesis deactivate at temperatures much in excess of 570 K [9,13] and the inlet gases to the synthesis reactor must be cooled, the exchanged heat being used to warm the reformer inlet feed. Since the conversion per pass is around 3% [9] recycle of the unconverted reactants is essential to give a total of 10% after recycle.

The cascade array is required also to produce synthesis gas at the same conditions but uses a different arrangement to produce the

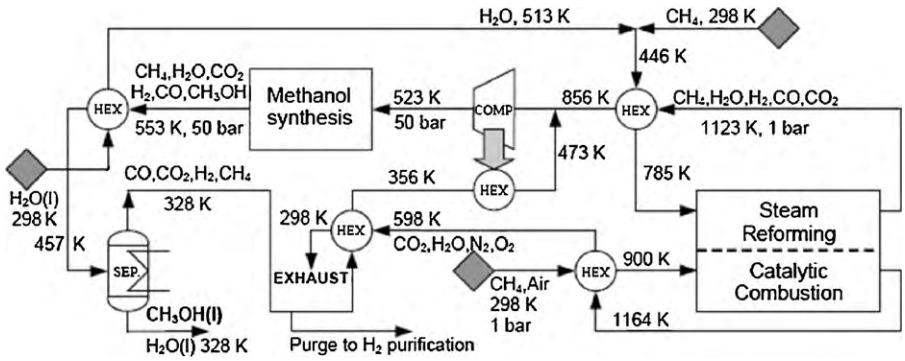

Fig. 1. Process flow diagram of methanol production.

methanol reactor feed [11]. Both steam reforming and catalytic combustion occur in separate multiple adiabatic beds with heat transfer involving parallel microchannels that connect the series of beds. Conversion in any one bed of the series is limited, often by the desired temperature change. This can present problem with catalytic combustion in that the system lights off easily and conversion should be limited to less than about 20% if temperature is to be controlled [14,15]. Alternatively catalytic combustion could be taken to completion in each individual bed, the flow of natural gas and air to each bed being adjusted to limit the heat generated.

Typical temperatures involved in the methanol synthesis are presented in Fig. 1. Inlet and exit temperatures of steam reforming, 785 K and 1123 K, respectively and the inlet temperature and pressure to the methanol synthesis reactor (523 K, 50 bar) are adapted from actual process practice reported in Ref. [9]. Temperature at the inlet of the catalytic combustion unit is set as the light-off temperature of methane, 900 K [14]. Temperature at the exit of the separator unit, 328 K, is set to be lower than the boiling point of methanol (338 K), so that all of the methanol could be obtained in the liquid phase. Finally, the inlet streams entering to the process and exhaust streams leaving the process (except methanol exit from the separator) are assumed to be at 298 K. Rest of the temperatures shown in Fig. 1 are calculated by mole and energy balances around the specific control volumes. The molar flow rates are calculated by the mole balances around the units by taking a basis of 1 kmol h^{-1} of methane entering into the steam reformer and by assuming 90% steam reforming conversion [9], complete conversion of methane in combustion [14], and the molar ratio of methane reformed-to-methane combusted as 3. The calculated flow rates are then adapted to the desired throughput by flowsheet scaling. These balance calculations are conducted by using ChemCad^{TM} process simulation software which can calculate the effluent properties of a unit provided that the properties of the inlet stream and the unit are defined. The necessary thermochemical data such as reaction enthalpy and heat capacity of the species are used directly from the database of ChemCad^{TM}.

In the case of ethane dehydrogenation, temperature control is essential to avoid coke deposition over the catalyst:

$$C_2H_6 = C_2H_4 + H_2 \qquad \Delta H^0_{298} = +136.9\,\text{kJ/mol} \tag{5}$$

The olefin-to-paraffin equilibrium is favoured only at high temperatures (ca. 1000 K) which also favour coking [16] and diluents, often used to minimise coking, tend to deactivate the catalysts. As a result, commercial processes are often based on a dehydrogenation–regeneration cycle, dehydrogenation being optimised when temperature control limits the coke formation. Since coking is particularly deleterious in microchannel systems and channel blockage can occur, minimisation of coking demands careful control of temperature which, in the microsystems, necessitates careful control of heat generated by the catalytic combustion. The process flow diagram for ethane dehydrogenation is much simpler than is the case for methanol (Fig. 2), in which the inlet streams entering to the process are assumed to be at 298 K, inlet temperature of the catalytic combustion unit is set as the light-off temperature of methane (900 K) [14], inlet and exit temperatures of ethane dehydrogenation is taken as 923 K and 1053 K, respectively [8] and the molar ratio of ethane dehydrogenated-to-methane combusted is set as 3. These values are being expected to be high enough to give reasonable conversions – 62% in reaction (5) [8] and ca. 100% in reaction (4) [14] – and low enough to avoid very significant coking. As explained in the case of methanol synthesis, other temperatures in Fig. 2 are calculated via the ChemCad^{TM} process simulation software.

Microchannel and cascade reactor configurations are compared in the synthesis gas generation part of the methanol synthesis process, where catalytic steam reforming (reactions (1) and (2)) and combustion of methane (reaction (4)) are coupled. The reactor configurations are also compared for methane combustion and ethane dehydrogenation (reaction (5)) coupling. The comparisons are made on the basis of computer-based modelling and simulation tools, whose details are presented in Section 3. The relative advantages of the reactor configurations for methanol synthesis and ethane dehydrogenation processes are discussed in Section 4.

3. Mathematical modelling

3.1. Microchannel reactor configuration

The geometry on which the representative microchannel model is to be implemented is given in Fig. 3. It involves a repeating unit

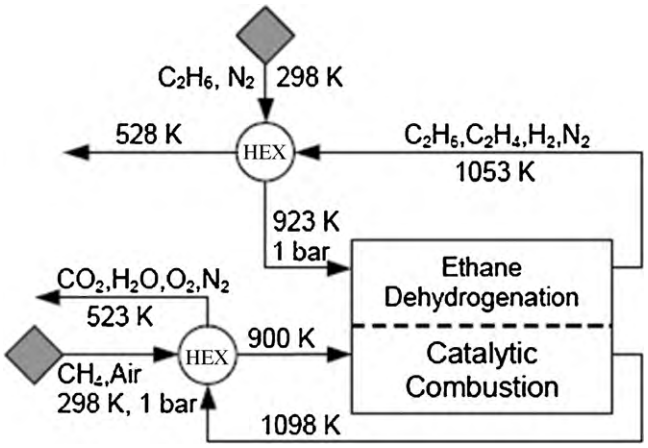

Fig. 2. Process flow diagram of ethane dehydrogenation.

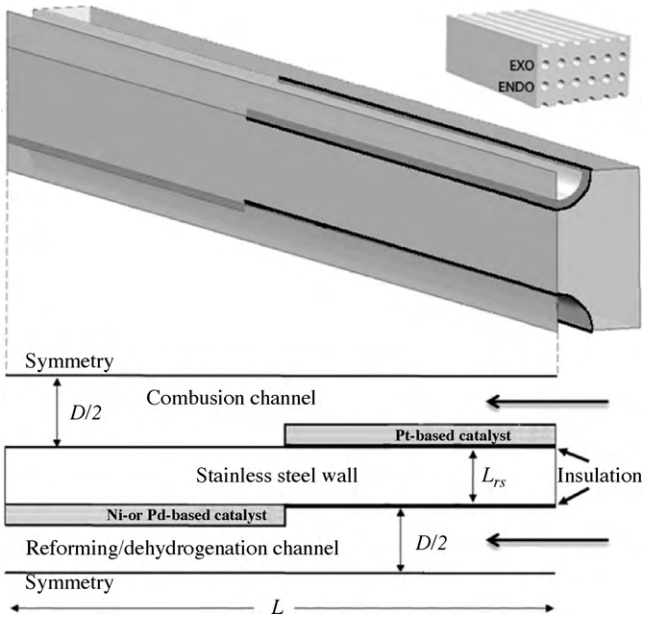

Fig. 3. Description of the microchannel configuration.

composed of the co-current flow of exothermic (methane combustion) and endothermic reaction (steam reforming or ethane dehydrogenation) streams in two parallel channels between which heat is transferred through the stainless steel wall. Due to the symmetry, the behaviour of this unit represents the response of the multichannel reactor in which the exothermic and endothermic channels are grouped in horizontal layers as shown in Fig. 3. The diameters of both channels in the repeating unit are taken as 280 μm. The porous, catalytic washcoat layers are assumed to be coated on the channel walls and their thickness are taken as 60 μm. The width of the separating wall, which is considered to be made of stainless steel, is taken as 400 μm. Length of the channels, i.e. the length of the reactor, is assumed to be 5 cm. In order to obtain desired steam reforming and ethane dehydrogenation conversion levels (>80% and >60%, respectively) and feed composition for the methanol synthesis, high temperatures in excess of 1100 K are needed. For this purpose, the fluid–wall interfaces are considered to be coated with a thin insulating layer along the first half of the channels (Fig. 3) and the insulated zones are assumed to behave in adiabatic mode. Moreover, the catalytic washcoats are considered to be applied only in the first half of the exothermic flow channel and in the second half of the endothermic flow channel as shown in Fig. 3. Such a scheme conserves the exothermal heat within the combustion channel to induce methane light-off and allows reaction (4) to proceed until the temperature in the endothermic channels rises to ca. 1200 K, as desired: our early simulations have shown that when the parallel channels were completely coated with catalysts and there were no insulations as shown in Fig. 3, endothermic reactions absorbed the exothermal heat generated by methane combustion immediately at the inlet (first 0.5 cm) of the channels, no methane light-off was observed and the maximum temperatures were below ca. 920 K that were insufficient to obtain the desired conversions of methane and ethane in reactions (1), (2) and (5), respectively. The presence of insulation in the combustion channel does not have any effect on the conduction of the generated heat in the axial direction of the catalytic layer and heat transfer to the gaseous phase, since the Pt-based catalyst is placed on top of the insulation (Fig. 3). It is worth noting that, in actual practice, it may not be possible to ensure perfect adiabatic conditions in the first half of the microchannels. However, the use of ceramics having thermal conductivities of ca. 10–20 times smaller than that of stainless steel may help in providing a thermal response at the near-adiabatic scale.

Even though the microchannel diameters are in the sub-millimeter range, temperature and concentration variation in the lateral direction have to be accounted for since the reactions take place in the wall-coated catalyst layers. Three-dimensional cylindrical models offer accuracy at the expense of increased computational cost, therefore, the two-dimensional axisymmetric model that neglects angular variations are employed in microchannel modelling. The steady-state mass, momentum and energy conservation equations are given in Table 1. The conservation of momentum is described by the Navier–Stokes equations including contributions both from diffusive and convective mechanisms. Brinkman equations are used to model flow in porous, catalytic washcoat media. Permeability and porosity of the washcoat layer are taken as 1×10^{-8} m^2 and 4×10^{-1}, respectively.

The thermal model involves the set of two-dimensional energy conservation equations because of heat conduction in the washcoat media and through the steel wall in series (Table 1). Axial conduction both in the gas and solid phases is also taken account due to their significance in microfluidic conditions. The rates of reactions are incorporated into the species mass transport equations through source terms. It should be noted that only heterogeneous reactions are considered; homogeneous gas-phase reactions are neglected. The model equations are solved using the finite element method through the Comsol Multiphysics™ CFD

Table 1
Model equations used to simulate the microchannel behaviour.

Gas phase

Continuity equation: $\frac{1}{r_j}\frac{\partial(r_j v_{rj})}{\partial(r_j)} + \frac{\partial v_{zj}}{\partial z_j} = 0$

Conservation of momentum:

$$\rho_j\left(v_{rj}\frac{\partial v_{rj}}{\partial r_j} + v_{zj}\frac{\partial v_{rj}}{\partial z_j}\right) = -\frac{\partial p_j}{\partial r_j} + \mu_j\left[\frac{\partial}{\partial r_j}\left(\frac{1}{r_j}\frac{\partial}{\partial r_j}(r_j v_{rj})\right) + \frac{\partial^2 v_{rj}}{\partial z_j^2}\right]$$

$$\rho_j\left(v_{rj}\frac{\partial v_{zj}}{\partial r_j} + v_{zj}\frac{\partial v_{zj}}{\partial z_j}\right) = -\frac{\partial p_j}{\partial z_j} + \mu_j\left[\frac{1}{r_j}\frac{\partial}{\partial r_j}\left(r_j\frac{\partial v_{zj}}{\partial r_j}\right) + \frac{\partial^2 v_{zj}}{\partial z_j^2}\right]$$

Species mass transport: $v_{rj}\left(\frac{\partial c_{ij}}{\partial r_j} + v_{zj}\frac{\partial c_{ij}}{\partial z_j}\right) = \mathcal{D}_{AB}\left[\frac{1}{r_j}\frac{\partial}{\partial r_j}\left(r_j\frac{\partial c_{ij}}{\partial r_j}\right) + \frac{\partial^2 c_{ij}}{\partial z_j^2}\right]$

Conservation of energy:

$$\rho_j C_{pj}\left(v_{rj}\frac{\partial T_j}{\partial r_j} + v_{zj}\frac{\partial T_j}{\partial z_j}\right) = \lambda_j\left[\frac{1}{r_j}\frac{\partial}{\partial r_j}\left(r_j\frac{\partial T_j}{\partial r_j}\right) + \frac{\partial^2 T_j}{\partial z_j^2}\right]$$

Washcoat phase

Continuity equation: $\frac{1}{r_j}\frac{\partial(r_j v_{rj})}{\partial r_j} + \frac{\partial v_{zj}}{\partial z_j} = 0$

Conservation of momentum:

$$\frac{\mu_j}{k}v_{rj} = -\frac{\partial p_j}{\partial r_j} + \left(\frac{\mu_j}{\epsilon_p}\right)\left[\frac{\partial}{\partial r_j}\left(\frac{1}{r_j}\frac{\partial}{\partial r_j}(r_j v_{rj})\right) + \frac{\partial^2 v_{rj}}{\partial z_j^2}\right]$$

$$\frac{\mu_j}{k}v_{zj} = -\frac{\partial p_j}{\partial z_j} + \left(\frac{\mu_j}{\epsilon_p}\right)\left[\frac{1}{r_j}\frac{\partial}{\partial r_j}\left(r_j\frac{\partial v_{zj}}{\partial r_j}\right) + \frac{\partial^2 v_{rj}}{\partial z_j^2}\right]$$

Species mass transport:

$$v_{rj}\left(\frac{\partial c_{ij}}{\partial r_j} + v_{zj}\frac{\partial c_{ij}}{\partial z_j}\right) = \mathcal{D}_{AB,eff}\left[\frac{1}{r_j}\frac{\partial}{\partial r_j}\left(r_j\frac{\partial c_{ij}}{\partial r_j}\right) + \frac{\partial^2 c_{ij}}{\partial z_j^2}\right] + R_{ij}$$

Conservation of energy: $\rho_j C_{pj}\left(v_{rj}\frac{\partial T_j}{\partial r_j} + v_{zj}\frac{\partial T_j}{\partial z_j}\right) = Q_j + \lambda_{j,eff}\left[\frac{1}{r_j}\frac{\partial}{\partial r_j}\left(r_j\frac{\partial T_j}{\partial r_j}\right) + \frac{\partial^2 T_j}{\partial z_j^2}\right]$

Solid phase

Conservation of energy: $\lambda_s\left[\frac{\partial^2 T_s}{\partial x_s^2} + \frac{\partial^2 T_s}{\partial y_s^2}\right] = 0$

j – Channel or washcoat
1. Combustion
2. Reforming or dehydrogenation

I – Species
$i_{(j=1)}$: CH_4, O_2, H_2O, CO_2, N_2
$i_{(j=2)}$: CH_4, H_2O, CO, H_2, CO_2 (steam reforming), C_2H_6, N_2, C_2H_4, H_2 (ethane dehydrogenation)

s – Wall

package. Unstructured meshing is employed and the mesh is refined in regions where high reaction rates are expected.

In the combustion channel, the multicomponent gas mixture consists of methane, oxygen, nitrogen, steam and carbon dioxide. The mixture in the steam reforming channel consists of methane, steam, carbon monoxide, hydrogen and carbon dioxide. Ethane dehydrogenation takes place in a mixture of ethane, nitrogen, hydrogen and ethylene. Since the reactions are carried out at atmospheric pressure, the gas mixtures are assumed to be ideal and incompressible Newtonian fluids. The flow is strictly in the laminar regime, i.e. $Re < 210$, which is one of the requirements for microchannel analysis. The species and mixture thermal conductivities and viscosities as functions of temperature are calculated using the correlations given in the literature [17]. The specific densities are estimated by the ideal gas equation of state. The species mass diffusivities are assumed to be identical and constant in the channels. Typical values of the gas phase and washcoat effective diffusivities calculated by Cao et al. [18], 1.8×10^{-5} m^2 s^{-1} and 5.35×10^{-7} m^2 s^{-1}, respectively, are used in the equations. Empirical values for the effective thermal conductivities in the washcoat phase are taken as 4.2 and 4.5 times the bulk fluid conductivity for the exothermic and endothermic reaction catalysts, respectively.

Ma and Trimm [14] determined the intrinsic kinetics of methane oxidation on a Pt/Al_2O_3 catalyst which is adopted for the methane combustion reaction in this work. The rate expressions proposed by Xu and Froment [19] are used to describe methane steam reforming and water–gas shift kinetics on a Ni/Al_2O_4 catalyst. The kinetics of ethane dehydrogenation on a Pd-based catalyst in the presence of nitrogen as sweep gas, which was modelled by Gobina et al. [20], is employed in evaluating the rate.

The governing equations given in Table 1 are solved subject to the boundary conditions given in Table 2 which takes the geometric considerations given in Fig. 3 into account. At the inlet of the flow domains, plug-flow velocities are assumed. No-slip condition is imposed on the impermeable walls of the channels and atmospheric pressure is specified at the outlets. Species concentrations are specified at the inlets while convective flux is assumed to be zero at the outlets. Gases at the inlets are preheated to the reaction temperatures and the exit boundary conditions are assumed to be of the convective type that are equal to zero. Conjugate heat transfer between the solid wall and the fluid flow in porous media is handled by means of heat flux continuity at the interface. For all types of transport phenomena, the symmetry condition is imposed, which is a prerequisite for the two-dimensional axisymmetric model.

Table 2
Boundary conditions used to solve model equations given in Table 1.

1. Channel entrance: $z_j = 0$; $\forall r_j$
   $U_j = U_j^0$
   $c_{ij} = c_{ij}^0$
   $T_j = T_j^0$

2. Symmetry at the centerline: $\forall z_j$; $r_j = \pm(L_{rs}/2 + D/2)$
   $\mathbf{n} \cdot \nu_j = 0$
   $\mathbf{n} \cdot (-\mathcal{D}_{AB} \nabla c_{ij} + c_{ij} \nu_j) = 0$
   $\mathbf{n} \cdot (-k_j \nabla T_j + \rho_j C_{pj} T_j \nu_j) = 0$

3. Along the fluid-solid wall interface: $\forall z_j$; $r_j = \pm L_{rs}/2$
   $\mathbf{n} \cdot \nu_j = 0$
   $\mathbf{n} \cdot (-\mathcal{D}_{AB} \nabla c_{ij} + c_{ij} \nu_j) = 0$

   3.1. Along the insulation at the fluid–wall interface: $0 \le z_j \le L/2$; $r_j = \pm(L_{rs}/2 + \in)$
   $\mathbf{n} \cdot (-k_j \nabla T_j + \rho_j C_{pj} T_j \nu_j) = 0$

4. Channel exit: $z_j = L$; $\forall r_j$
   $p_j = p_{out}$
   $\mathbf{n} \cdot (-\mathcal{D}_{AB} \nabla c_{ij}) = 0$
   $\mathbf{n} \cdot (-k_j \nabla T_j) = 0$

5. Solid boundaries: $z_s = 0$ and $Z_s = L$; $\forall r_s$
   $\mathbf{n} \cdot (-k_s \nabla T_s) = 0$

3.2. Cascade reactor configuration

The cascade design procedure is primarily of a trial-and-error nature. Starting with given sizes of adiabatic packed beds in the exothermic and endothermic reaction arrays, the outlet temperatures from each bed pair are determined. The inlet temperatures to the subsequent pair are then assigned, which also dictates the amount of interstage heat exchange. The procedure is repeated until the number of bed pairs sufficient to achieve the desired reactant conversion is known. If certain process constraints are violated or desired conversion cannot be achieved in an acceptable number of stages using the given configuration, the process is reiterated by varying the assumed bed sizes and amount of interstage heat exchange.

Among the constraints the most restrictive one is the upper allowable limit of methane combustion conversion, 20% [14,15], the exceeding of which creates conditions that lead to thermal runaway and make it impossible to control the temperature precisely. Yet another but less stringent constraint is the aspect ratio of the beds which dictates that the length-to-diameter ratio be in an acceptable range and that the pressure drop not be so high as to permit process infeasibilities. Thus, the reactors should be sized such that combustion conversion and pressure drop in each bed are limited to 20% and 1%, respectively. A one-dimensional pseudohomogeneous reactor model is used for the simulation of the adiabatic operation in fixed-bed reactors. The working equations are

$$\frac{dF_{ij}}{dW_j} = R_{ij} \tag{6}$$

$$\frac{dT_j}{dW_j} = \frac{\sum_k (-\Delta H_k r_k)}{\sum_i F_i c_{pi}} \tag{7}$$

$$\frac{dp_j}{dW_j} = -\frac{\beta_0}{A_c \rho_{bj}} \frac{p_{j0}}{p_j} \frac{T_j}{T_{j0}} \frac{F_{Tj}}{F_{Tj0}} \tag{8}$$

with the initial conditions

$$F_{ij} = F_{ij0}, \quad T_j = T_{j0}, \quad p_j = p_{j0} \qquad \text{at} \quad W_j = 0 \tag{9}$$

The notation is similar to that used in microchannel modelling such that i denotes the species, j, the exothermic or endothermic operation line, and k, the particular reaction in each line. Rate expressions are the same as those for microchannel calculations. The resulting set of ordinary differential equations is solved using a stiff solver (ode15s) in the MATLAB™ environment.

The design of microchannel heat exchangers connecting the catalytic beds differs slightly from microchannel reactor design in that the set of equations given in Table 1 governing gas-phase transport alone are considered due to the absence of catalytic porous media. Comsol Multiphysics™ CFD package is used for solving the equations. Absence of the source terms allowed solution of the equations with lower computational times as a result of coarser meshing. The representative unit cell of the heat exchanger involves co-current flow of hot and cold streams in adjacent channels in which heat is transferred through the stainless steel wall. The variables available for adjustment are the length and channel diameters. Inasmuch as heat loads at the

intermediate exchange stages are variable, design is suited to the highest one.

In the case of microchannel heat exchangers and microreactor configuration, any given channel is part of an array of channels, each of which has the same reaction occurring within. For example, heating and cooling channels in the microchannel heat exchangers of the cascade system (or the combustion and steam reforming/dehydrogenation channels in the microreactor configuration) are placed as groups in successive rows as shown in Fig. 3. As a result heat loss between the channels of the same row will be minimal except at the outermost channels. Since these are only a small percentage of the whole, a general assumption is made that the heat losses from heat exchangers and microreactors are negligible.

Sizing, i.e. numbering up of the catalytic microchannels, is handled by dividing the basis flow rates with the corresponding single-channel flow rates given in Section 4. Sizing of the microchannel heat exchangers in the cascade configuration is done by dividing the total flow leaving each reactor by flow through a single pair of channels and finding the number of channels that meets the actual load. Owing to the interstage temperatures that are determined during the phase of sizing and numbering of catalytic beds, the heat load is known prior to design. Flow through a single pair of microchannels or equivalently, the number of microchannels is assumed initially. With the channel dimensions set, the transport equations are solved using the Comsol Multiphysics™ package as explained above. The dimensions, i.e. diameter and length, are varied until the exit criteria are met. If the acceptable set of diameter and length combinations cannot meet the exit temperature and pressure criteria, the number of channels is changed and the procedure is started all over again. Sizes of the microchannel and cascade configurations are compared on the basis of 1000 std. $m^3\ day^{-1}$ of methane being fed to steam reforming. In the case of ethane dehydrogenation, the basis is set as 1000 std. $m^3\ day^{-1}$ of ethane being fed to the dehydrogenation reaction.

4. Results and discussion

Initial modelling is carried out to simulate methane combustion/methane steam reforming coupling in the parallel microchannel configuration, shown in Fig. 3. The amount of methane fed and the feed compositions are optimised to obtain the desired inlet feed composition for the methanol synthesis, which is H_2:CO:CO_2 = 75:24:1 per cent by mole at the exit of steam reforming [9]. Methane feeds to the combustion and steam reforming channels are set at 4×10^{-7} mol s^{-1} and 1.24×10^{-6} mol s^{-1}, respectively. The molar inlet flow of oxygen in air is set at 8×10^{-7} mol s^{-1}, and the amount of steam fed to the steam reforming channel is assigned as 3.1×10^{-6} mol s^{-1} to come up with an inlet steam-to-carbon ratio of 2.5, which is reported to minimise coke formation over Ni-based catalysts [10]. As demonstrated in the process flowsheet given in Fig. 1, feed temperatures of the combustion and steam reforming channels are taken as 900 K and 785 K, respectively. The results of the microchannel simulations are presented in Fig. 4 and in Table 3. It can be seen that the temperature in the combustion channel is raised from 900 K to ca. 1290 K as a result of oxidation of 88% of the methane fed (Fig. 4 and Table 3) over the Pt-based catalyst which is coated in the first half of the channel (Fig. 3). The insulation in this zone disabled heat transfer into the metallic wall and prevented any reductions in the temperature of the combustion stream. The second half of the combustion channel, on the other hand, involves neither catalyst nor insulation. As a result no chemical reactions took place due to the assumed absence of the homogeneous reactions (Section 3.1) and heat generated in the catalytic zone is transferred to the steam reforming channel. This has led to a sharp rise in the steam reforming stream temperature from 785 K to 1225 K, accompanied with a ca. 100 K overshoot despite the presence of reactions (1) and (2) running in the second half of the channel coated with Ni-based catalyst (Fig. 4 and Table 3). Such a thermal response may lead to local, temperature-induced problems in catalytic operation, though it will not disturb the nature of the stainless steel. The endothermicity of methane steam reforming (reactions (1) and (2)) then started to dominate and triggered a decreasing trend in temperature to give an exit value of 1125 K. The small dimension and metallic nature of the separating wall facilitated rapid heat transfer and allowed the temperatures of both streams to equilibrate immediately (Fig. 4 and Table 3).

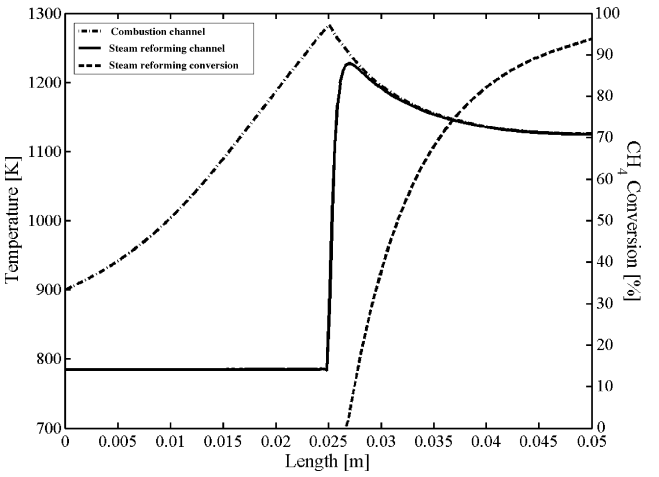

Fig. 4. Simulation results of methane combustion–methane steam reforming coupling in the microchannel configuration.

The high temperatures brought by combustion gave 95% steam reforming conversion of methane and an exit stream including 3.21×10^{-6} mol s^{-1} H_2, 1.07×10^{-6} mol s^{-1} CO and 5.6×10^{-10} mol s^{-1} CO_2 with a H_2:CO ratio of 3, which is close to the desired reforming exit composition given above. The small amount of CO_2 reflects the importance of the reverse water gas shift reaction ($CO_2 + H_2 = CO + H_2O$, $\Delta H^0_{298} = +41.2$ kJ/mol) at high temperatures. The analysis of the outlet from the steam reformer shows that

Table 3
Comparison of the results of microchannel and cascade systems for coupled methane combustion–methane steam reforming reactions.

		Inlet[a]				Outlet[b]					SR, T_{max} (K)	Total volume (m^3)	Total volume per syngas produced (m^3 mol^{-1})
		CH_4 (mol s^{-1})	O_2 (mol s^{-1})	H_2O (mol s^{-1})	T_0 (K)	x_{HC} (%)	H_2 (mol s^{-1})	CO (mol s^{-1})	CO_2 (mol s^{-1})	T (K)			
Microchannel	COMB	4×10^{-7}	8×10^{-7}	–	900	88	–	–	3.52×10^{-7}	1125	1225	17.7×10^{-3}	10.8×10^{-3}
	SR	1.24×10^{-6}	–	3.1×10^{-6}	785	95	3.21×10^{-6}	1.07×10^{-6}	5.6×10^{-10}	1125			
Cascade	COMB	0.21	0.42	–	900	80	–	–	0.167	1184	1032	8.2×10^{-3}	4.1×10^{-3}
	SR	0.473	–	1.18	785	91	1.50	0.52	3×10^{-4}	949			

[a] Molar flow rate of N_2 is not shown.
[b] Molar flow rates of N_2, H_2O and unreacted CH_4 are not shown.

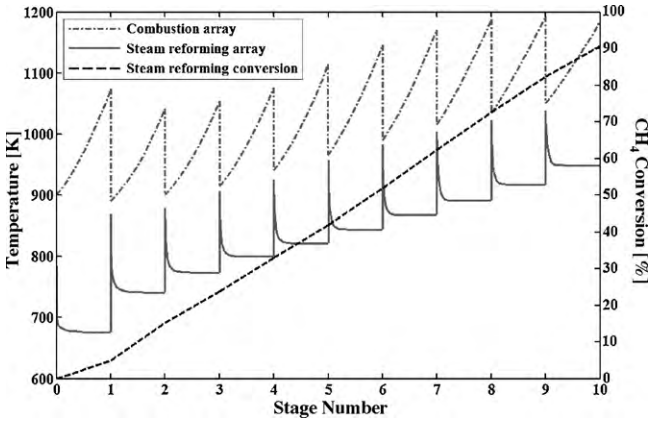

Fig. 5. Simulation results of methane combustion–methane steam reforming coupling in the cascade configuration.

conditions desired for the inlet of the methanol synthesis system can be easily achieved, although cooling of the exit gases is necessary before the methanol synthesis.

Coupling of methane combustion/methane steam reforming in the cascade reactor configuration is modelled using the same kinetic data [14,19]. Heat generated in a catalytic combustion bed is transferred to the steam reforming gas stream through a microchannel heat exchanger. The cooled stream is then fed to the next combustion bed to generate heat for steam reforming. The extent of the conversion in the combustion beds is limited to less than 20% in order to avoid any uncontrolled temperature rise due to the light-off. The heated reformer stream is then taken to the next catalytic bed in which further reforming conversion takes place adiabatically to give a decreasing trend in the temperature. Such heating–cooling cycles lead to saw tooth temperature profiles along the combustion and reforming arrays which are shown in Fig. 5. Evolution of the cumulative methane conversion along the steam reforming beds and the product flow rates are given in Fig. 5 and Table 3, respectively. The effluent of the steam reforming beds having a molar H_2:CO ratio of 2.86 (Table 3) shows that the inlet stream desired for the methanol synthesis can also be obtained through the cascade array with the advantage of a much better temperature control (Figs. 4 and 5): although the inlet temperatures are the same (Table 3), the maximum steam reforming temperatures obtained in the microchannel and in the cascade configurations are 1225 K and 1032 K, respectively. The absence of any uncontrolled temperature elevations in the cascade array minimises the risk of catalyst deactivation due to thermal effects.

The desired conversion/product distribution values and well-controlled temperature are achieved by the use of 10 catalytic beds per gas stream, summing up to a total of 20 catalytic beds. The number of beds is optimal, since the use of lower number of beds requires disturbing the methane combustion conversion constraint of 20% per bed to achieve the same effluent properties, whereas using higher number of beds brings only incremental improvements in conversion. Comparison of the output of the two configurations in Table 3 shows that the overall size of the cascade system needed to produce unit amount of product is smaller than that of the microchannel arrangement, with the steam reforming conversion slightly higher in the latter due to the higher temperatures. In addition, the ease of replacement of the catalysts in the cascade system, once they deactivate, is a real advantage. This system is also beneficial in the sense that the cooling duty and heat exchanger size needed for cooling the steam reforming exit stream to the methanol synthesis conditions is lower than needed in a microchannel system. This is due to the exit temperature of the cascade system, 949 K, which is significantly lower than that of the microchannel configuration, 1125 K (Table 3).

The two configurations are compared in another reaction system in which methane combustion is coupled with ethane dehydrogenation (reaction (5)). Temperature control is much more significant in the case of ethane dehydrogenation, where excessive coking must be avoided, despite the high temperatures involved [16]. Heat from catalytic combustion is provided directly to the dehydrogenation reaction, which is operated at ca. 1000 K (Fig. 2). Simulation of catalytic combustion in the microchannel array is conducted using the same rate law [14] employed in the case of combustion/steam reforming coupling. Ethane dehydrogenation is modelled using the kinetic data reported by Gobina et al. [20], a value of 65% conversion to ethylene forming the basis of the calculation. In order to minimise the risk of coking that may be favoured at temperatures in excess of ca. 1000 K, the desired inlet molar flow rate of ethane, 1.16×10^{-6} mol s^{-1}, is mixed with a diluent, N_2, to give a molar feed ratio of C_2H_6:N_2 = 4 [16]. Using N_2 at such a feed ratio will not cause catalyst deactivation; similar studies involving the same reaction coupling/catalyst combination did not report catalyst deactivation even though higher amounts of N_2 were used give C_2H_6:N_2 = 1 [21]. The heat required to drive reaction (5) is found to be produced from the combustion of 5.2×10^{-7} mol s^{-1} of methane in air, with an oxygen flow rate of 1.04×10^{-6} mol s^{-1}. As shown in the process flowsheet (Fig. 2), the feed temperatures of combustion and dehydrogenation channels are set at 900 K and 923 K, respectively. The geometric and structural properties of the parallel microchannels are exactly the same as given in Fig. 3 and defined in Table 2.

Simulated profiles of temperature in the microchannels and ethane conversion are presented in Fig. 6 and the related numerical results are given in Table 4. The trends of the profiles are in accordance with the assigned microchannel geometry as explained in the case of combustion/steam reforming coupling. Temperature rise along the dehydrogenation channel caused by catalytic combustion of 94% of the methane fed followed the expected increase, passing through a maximum of 1180 K as the cooling effect of dehydrogenation became apparent (Fig. 6 and Table 4). The lower heat of reaction of the endothermic dehydrogenation caused a smaller decrease in temperature (ca. 60 K, Fig. 6) than that associated with steam reforming and gave an exit temperature of 1120 K. The 65% conversion of ethane achieved reflects the dominating effect of thermodynamics of the reaction at the exit conditions, since it is limited by an equilibrium conversion of 72% [16].

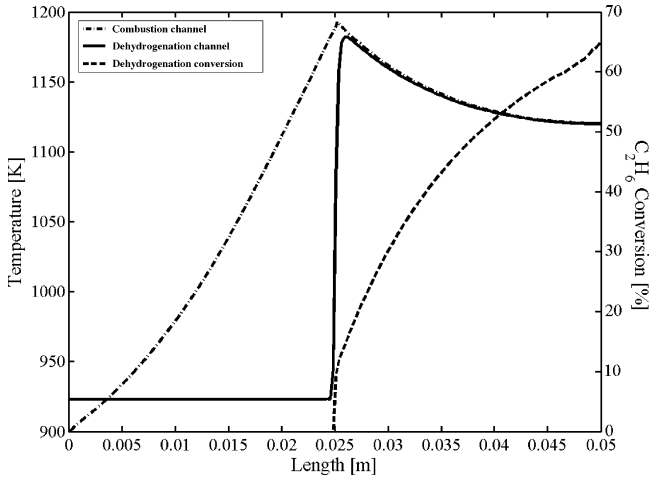

Fig. 6. Simulation results of methane combustion–ethane dehydrogenation coupling in the microchannel configuration.

Table 4
Comparison of the results of microchannel and cascade systems for coupled methane combustion–ethane dehydrogenation reactions.

		Inlet				Outlet[a]					ED, T_{max} (K)	Total volume (m^3)	Total volume per C_2H_4 produced (m^3 mol^{-1})
		HC (mol s^{-1})	O_2 (mol s^{-1})	N_2 (mol s^{-1})	T_0 (K)	x_{HC} (%)	C_2H_4 (mol s^{-1})	H_2 (mol s^{-1})	N_2 (mol s^{-1})	T (K)			
Microchannel	COMB	5.2×10^{-7}	1.04×10^{-6}	3.9×10^{-6}	900	94	–	–	3.9×10^{-6}	1120	1180	18.9×10^{-3}	61.8×10^{-3}
	ED	1.16×10^{-6}	–	2.9×10^{-7}	923	65	7.5×10^{-7}	7.5×10^{-7}	2.9×10^{-7}	1120			
Cascade	COMB	0.1	0.2	0.752	900	86	–	–	0.752	1245	1121	3×10^{-3}	10.2×10^{-3}
	ED	0.473	–	0.118	923	63.6	0.3	0.3	0.118	1054			

[a] Molar flow rates of CO_2, H_2O and unreacted hydrocarbons (CH_4 and C_2H_6) are not shown.

The results of methane combustion/ethane dehydrogenation in the cascade configuration are given in Fig. 7 and Table 4. The familiar saw tooth temperature pattern is observed both in the combustion cascade and in the dehydrogenation cascade (Fig. 7) and the increase in temperature of dehydrogenation occurs only from heat exchange with hot combustion gases. As explained in Section 3.2, temperatures in the combustion beds are controlled by allowing only 20% conversion per bed, in order to avoid light-off. Although the 86% conversion of methane was lower than obtained in the microchannel combustion (94%), efficient heat transfer through the microheat exchangers has led to improved temperature control in the dehydrogenation channel with almost no sacrifice from the overall ethane conversion, which is found to be 63.6% (Fig. 7 and Table 4). As expected, the maximum temperature of 1121 K obtained in the dehydrogenation cascade array is lower than 1180 K of the corresponding microchannel array. As in the case of combustion/steam reforming coupling, the optimum number of cascades per gas stream that delivered the responses above is found to be 10.

Based on the flow rates in a single pair of channels in the microreactor configuration, the total number of microchannels for the steam reforming system is 763,000 whereas that for ethane dehydrogenation is 816,000. Given the system specifications in Section 3.1, the microreactor volumes for steam reforming and ethane dehydrogenation are 17.7×10^{-3} m^3 and 18.9×10^{-3} m^3, respectively (Tables 3 and 4).

The catalyst beds in the cascade configuration are designed for ease of placement, therefore, they are assumed to be of the same length. The hydraulic diameter and length of each of the 10 combustion beds used in the steam reforming system are 8.25×10^{-2} m and 4.13×10^{-2} m, respectively. The Pt-based catalyst loading is 0.245 kg. The diameter and length of the combustion beds used in ethane dehydrogenation are 6.22×10^{-2} m and 3.11×10^{-2} m, which amount to 0.105 kg of catalyst. Each of the steam reforming reactors has 12.75×10^{-2} m diameter and 4.13×10^{-2} m length, and contains 0.635 kg of Ni-based catalyst. One dehydrogenation reactor is 8.93×10^{-2} m in diameter and 3.11×10^{-2} m in length. The Pd-based catalyst loading is 0.235 kg.

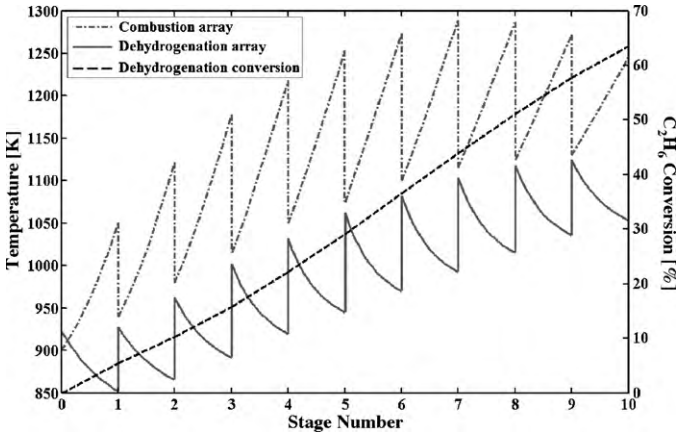

Fig. 7. Simulation results of methane combustion–ethane dehydrogenation coupling in the cascade configuration.

Dimensions of the interconnecting microchannel heat exchangers for the steam reforming and dehydrogenation cascade configurations, based on the largest amount of interstage heat exchange, are $(H = 4.83, W = 3.76, L = 4.50) \times 10^{-3}$ m and $(H = 3.03, W = 3.01, L = 2) \times 10^{-3}$ m, respectively. The heat exchangers used in dehydrogenation house a total of 10,000 channels while those used in steam reforming have 20,000 channels. The 200-μm diameter channels are separated by 100-μm thick stainless steel walls.

Comparison of the results of the two systems given in Table 4 shows that, the size of the cascade system, including the heat exchangers, needed to produce unit amount of ethylene is smaller than that of the microchannel system, whereas the conversions of both ethane and methane are higher in the latter configuration. However the advantage of easy replacement of deactivated catalyst in the cascade system, coupled to better temperature control to minimise the risk of temperature-induced coking, are real benefits.

5. Conclusions

The performances of two intensified catalytic reactor configurations, parallel microchannels and cascades, are compared in the contexts of synthesis gas generation for methanol synthesis and of ethylene production by non-oxidative dehydrogenation of ethane using computer-based modelling techniques. Both of the processes involve heat transfer between an exothermic (methane combustion) and an endothermic reaction (methane steam reforming or ethane dehydrogenation) and require careful temperature control. It is clear that either reactor system is capable of meeting the desired conversion/product distribution demands and show clear advantages over conventional processing for smaller scale operations. Feedstock conversions in steam reforming and in dehydrogenation are observed to be slightly higher in the microchannel arrangement. On the other hand, temperature control is found to be much better in the cascade system such that presence of sharp temperature elevations and peaks that can increase the risk of thermal degrading of the catalysts are eliminated. The cascade system is also found to be smaller than the microchannel configuration. The ability to remove deactivated catalyst from the reactors easily and the ability to decouple reaction kinetics from heat exchange make the cascade system a promising alternative.

Acknowledgments

David L. Trimm thanks Boğaziçi University for very real hospitality during sabbatical leave. Ahmet K. Avcı acknowledges Boğaziçi University Research Fund project BAP-06A503 and TUBITAK-MAG project 108M509.

References

[1] R.S. Benson, J.W. Ponton, Chem. Eng. Res. Des. 71 (1993) 160.
[2] V. Hessel, H. Löwe, A. Müller, G. Kolb, Chemical Micro Process Engineering: Processing and Plants, Wiley-VCH, Weinheim, 2005, p. 385.
[3] L. Kiwi-Minsker, A. Renken, Catal. Today 110 (2005) 2.
[4] R. Zapf, C. Becker-Willinger, K. Berresheim, H. Holz, H. Gnaser, V. Hessel, G. Kolb, P. Löb, A.K. Pannwitt, A. Ziogas, Trans. IChemE A81 (2003) 721.
[5] Y. Wang, Y.H. Chin, R.T. Rozmiarek, B.R. Johnson, Y. Gao, J. Watson, A.Y. Tonkovich, D.P. Vander Wiel, Catal. Today 98 (2004) 575.
[6] A.Y. Tonkovich, B. Yang, S.T. Perry, S.P. Fitzgerald, Y. Wang, Catal. Today 120 (2007) 21.
[7] J. Frauhammer, G. Eigenberger, L. von Hippel, D. Arntz, Chem. Eng. Sci. 54 (1999) 3661.
[8] M. Zanfir, A. Gavriilidis, Chem. Eng. Sci. 58 (2003) 3947.
[9] G.W. Bridger, M.S. Spencer, in: M.V. Twigg (Ed.), Catalyst Handbook, 2nd edn., Wolfe Publishing Ltd., London, 1989, p. 441.
[10] J.R. Rostrup-Nielsen, in: J.R. Anderson, M. Boudart (Eds.), Catalysis, Science and Technology, vol. 5, Springer, Berlin, 1984, p. 3.
[11] E.L.C. Seris, G. Abramowitz, A.M. Johnston, B.S. Haynes, Chem. Eng. J. 135S (2008) S9.
[12] E.L.C. Seris, G. Abramowitz, A.M. Johnston, B.S. Haynes, Chem. Eng. Res. Des. 83 (A6) (2005) 619.
[13] D.L. Trimm, Appl. Catal. 7 (1983) 249.
[14] L. Ma, D.L. Trimm, C. Jiang, Appl. Catal. A: Gen. 138 (1996) 275.
[15] A.K. Avcı, D.L. Trimm, Z.I. Önsan, Chem. Eng. Sci. 56 (2001) 641.
[16] R.K. Kearby, in: P.H. Emmett (Ed.), Catalysis, vol. 3, Reinhold, New York, 1955 , p. 453.
[17] H.F. Rase, Fixed-bed Reactor Design and Diagnostics, Butterworths, Massachusetts, 1990, p. 75.
[18] C. Cao, Y. Wang, R.T. Rozmiarek, Catal. Today 110 (2005) 92.
[19] J. Xu, G.F. Froment, AIChE J. 35 (1989) 88.
[20] E. Gobina, K. Hou, R. Hughes, Chem. Eng. Sci. 50 (1995) 2311.
[21] M. Zanfir, A. Gavriilidis, Chem. Eng. Sci. 56 (2001) 2671.